J. Fluid Mech. (2019), *vol.* 874, *pp.* 548–572.
doi:10.1017/jfm.2019.466

Coupled fluid and energy flow in fabrication of microstructured optical fibres

Yvonne M. Stokes[1,†], **Jonathan J. Wylie**[2,3] **and M. J. Chen**[1]

[1]School of Mathematical Sciences and Institute for Photonics and Advanced Sensing, The University of Adelaide, SA 5005, Australia

[2]Department of Mathematics, City University of Hong Kong, Kowloon, Hong Kong SAR

[3]Center for Applied Mathematics and Statistics, New Jersey Institute of Technology, Newark, NJ 07102, USA

(Received 25 October 2018; revised 6 June 2019; accepted 6 June 2019; first published online 11 July 2019)

We consider the role of heating and cooling in the steady drawing of a long and thin viscous thread with an arbitrary number of internal holes of arbitrary shape. The internal holes and the external boundary evolve as a result of the axial drawing and surface-tension effects. The heating and cooling affects the evolution of the thread because both the viscosity and surface tension of the thread are assumed to be functions of the temperature. We use asymptotic techniques to show that, under a suitable transformation, this complicated three-dimensional free boundary problem can be formulated in such a way that the transverse aspect of the flow can be reduced to the solution of a standard Stokes flow problem in the absence of axial stretching. The solution of this standard problem can then be substituted into a system of three ordinary differential equations that completely determine the flow. We use this approach to develop a very simple numerical method that can determine the way that thermal effects impact on the drawing of threads by devices that either specify the fibre tension or the draw ratio. We also develop a numerical method to solve the inverse problem of determining the initial cross-sectional geometry, draw tension and, importantly, heater temperature to obtain a desired cross-sectional shape and change in cross-sectional area at the device exit. This precisely allows one to determine the pattern of air holes in the preform that will achieve the desired hole pattern in the stretched fibre.

Key words: capillary flows, lubrication theory

1. Introduction

Microstructured optical fibres (MOFs) are long and thin glass fibres that are typically approximately 150 μm in diameter and more than a kilometre in length. They contain a pattern of cylindrical air holes that run parallel to the axis of the fibre. To obtain a desired set of optical properties, the holes are required to have specific shapes and to be arranged in a particular pattern. This paper is concerned with the fluid mechanics of the fabrication of such fibres.

†Email address for correspondence: yvonne.stokes@adelaide.edu.au

Fibres are drawn from a preform that is typically 1–3 cm in diameter and 10–20 cm in length. One of the major challenges in drawing MOFs is to determine the pattern of air holes that must be in the preform in order to achieve the desired hole pattern in the stretched fibre. The process is further complicated by the fact that significant amounts of heat are required during the drawing process to allow extension with moderate stretching forces. These thermal variations give rise to enormous variations in the viscosity of the glass during the drawing process. Thermal variations also give rise to variations in the surface-tension coefficient that are less dramatic than the variations in viscosity, but can nevertheless be significant. We will therefore develop a coupled flow and temperature model that describes the evolution of the shapes of the holes and the external boundary during the drawing process for fluids with temperature-dependent viscosity and surface tension. Despite the apparent complexity of the problem, we will show that the evolution can be obtained using a straightforward solution procedure.

The drawing of viscous threads has an extensive history with the pioneering work dating back to Matovich & Pearson (1969). Much of the early work considered solid threads (with no holes) in an isothermal setting and a review of the early work can be found in Denn (1980). For axisymmetric threads in an isothermal setting, a huge amount of work has been done in recent years. Kaye (1991) devised a methodology to solve time-dependent extensional problems. A systematic derivation for extensional flows was undertaken by Dewynne, Ockendon & Wilmott (1992) and the analysis was generalised to include the effects of inertia and surface tension by Dewynne, Howell & Wilmott (1994). Yarin, Gospodinov & Roussinov (1994) developed a theory for the drawing of axisymmetric hollow tubes. Stokes *et al.* (2000) solved the problem of an inertialess solid thread falling under its own weight, inertial effects were included by Stokes & Tuck (2004), a very accurate numerical method was developed by Bradshaw-Hajek, Stokes & Tuck (2007) and the effects of surface tension were included by Stokes, Bradshaw-Hajek & Tuck (2011). Asymptotic solutions in the case with inertia were obtained for a thread extended by pulling with a fixed force at its ends by Wylie, Huang & Miura (2011), for a thread falling under gravity by Wylie, Huang & Miura (2015) and for a thread whose ends are pulled with a prescribed speed by Wylie, Bradshaw-Hajek & Stokes (2016). All of the above studies neglect thermal effects and are for axisymmetric threads, and therefore cannot be applied to MOFs that are subject to significant heating and have multiple holes.

Thermal effects for axisymmetric threads were first considered by Shah & Pearson (1972*a*,*b*) who examined how axial temperature variation affects stability of drawing. Further results for non-isothermal drawing were developed by Yarin (1986) who considered how cooling affects unsteady extension. Gupta & Schultz (1998) developed asymptotic corrections to the one-dimensional models that arise in the long and slender asymptotic limit. Forest & Zhou (2001) considered the sensitivity of drawing to transient fluctuations in the boundary conditions. Fitt *et al.* (2002) developed a theory for heated axisymmetric tubes and carefully considered various asymptotic limits. Wylie & Huang (2007) included the effects of viscous heating in unsteady extensional flows. Wylie, Huang & Miura (2007) showed that non-uniqueness can occur if sufficiently large viscosity variations occur during the drawing process. Suman & Kumar (2009) examined how draw ratio enhancement is affected by heating. Taroni *et al.* (2013) considered the relative importance of radiation, convection and conduction in the heating and cooling phases of glass drawing. He *et al.* (2016) considered the evolution of a solid thread composed of a material whose viscosity and surface tension depend on temperature. All of these studies focussed on axisymmetric threads and so cannot be applied directly to MOFs that have multiple holes.

A number of authors have considered the non-axisymmetric case. Cummings & Howell (1999) considered isothermal drawing for a solid thread with arbitrary shape and developed a novel transformation and Lagrangian solution procedure to determine the evolution of the shape of the thread. Griffiths & Howell (2007, 2008) used similar techniques for a non-axisymmetric thread with a single hole and considered the limit of slender thin-walled tubes. Remarkably, they obtained an explicit solution for the shape of a thread with arbitrary initial cross-section. The problem of multiple holes was also studied by Stokes *et al.* (2014). They considered the case in which the surface tension coefficient does not depend on temperature and showed that, if one can tune the pulling tension to a required value (for example, by varying the heater temperature), then, surprisingly, one can obtain the shapes of the holes at the exit of a draw tower without any detailed knowledge of the temperature or viscosity profile in the device. This work was extended to include the effects of active channel pressurisation by Chen *et al.* (2015). Buchak *et al.* (2015) developed a technique to regularise the inverse problem and gravitational extension and extrusional flows were considered by Tronnolone *et al.* (2016) and Tronnolone, Stokes & Ebendorff-Heidepriem (2017).

However, for threads fabricated from fragile materials, measuring the fibre tension is problematic and hence the procedure of obtaining the shapes of the holes at the exit without any detailed knowledge of the temperature (Stokes *et al.* 2014) cannot be applied. In addition, if the surface-tension coefficient depends on the temperature, the procedure also cannot be applied. So, in either of these cases, one must explicitly solve the thermal problem. One must also solve the thermal problem if one requires detailed information about the geometry of the thread in the draw tower rather than just the shape at the exit. For these reasons, we develop a fully coupled flow and temperature model that can describe the evolution of the thread and the holes throughout the drawing process. We show that, under a suitable transformation, the transverse motion of the thread decouples from the axial flow. The transverse flow can therefore be solved using standard techniques for Stokes flow problems in the absence of axial stretching. Having obtained the solution of the transverse-flow problem, one can then simply solve a system of three ordinary differential equations that completely determine the flow.

2. Model formulation

2.1. *Full three-dimensional model*

We consider a drawing device that feeds a thread of a viscous fluid (e.g. silica glass) with temperature θ_{in} through an aperture with a constant speed U_{in}. We denote the square root of the cross-sectional area of the fluid as it comes through the aperture as χ_{in}. At a distance L from the aperture, the thread is pulled by a take-up roller such that the thread has a speed U_{out}. When it passes through the aperture, the thread has a pattern of N internal air channels (see figure 1). Between the aperture and a distance $L_h < L$, the thread is exposed to a radiative heater. Between the end of the heater and the take-up roller, the thread experiences radiative heat loss to the environment. Throughout the entire length of the thread, convective cooling also occurs as a result of a forced flow of cold gas through the device around the deforming thread.

MOFs are typically composed of glass or polymeric materials and these both have the property that their density, specific heat and conductivity do not change significantly with temperature. We therefore assume that they are all constant. On the other hand, the viscosity of these materials changes dramatically with temperature. Variations of the surface-tension coefficient with temperature are typically not as

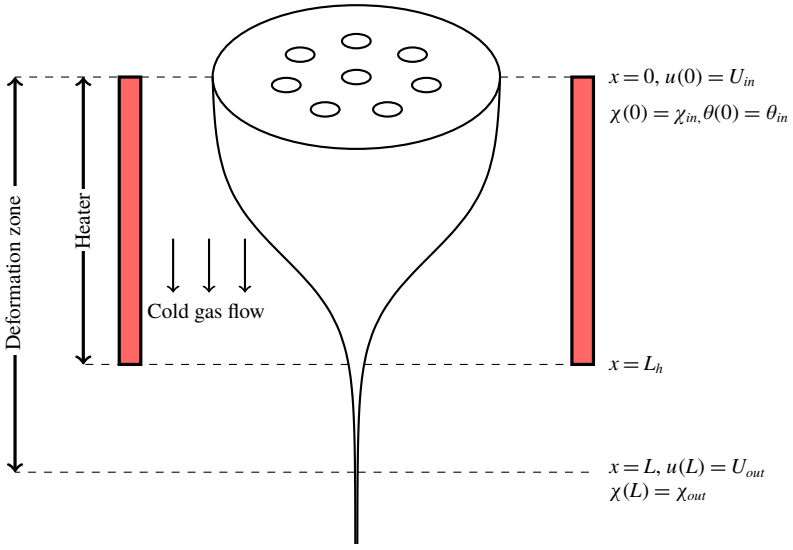

FIGURE 1. (Colour online) Schematic diagram of the neck-down region $0 \leqslant x \leqslant L$.

significant as variations in viscosity, but can nevertheless be significant (He *et al.* 2016).

We define a coordinate system with the x-axis directed along the axis of the thread. We take $x = 0$ to be the location of the aperture and y and z to be the coordinates in the cross-sectional plane. We denote the velocity vector, pressure and temperature by $\boldsymbol{u} = (u, v, w)$, p and θ, respectively. All of these dependent variables are, in general, functions of position $\boldsymbol{x} = (x, y, z)$ and the time that we denote as t. We denote the shape of the external boundary of the thread by $G^{(0)}(x, y, z, t) = 0$ and the shape of each of the N internal holes to be $G^{(i)}(x, y, z, t) = 0$, $i = 1, 2, \ldots, N$. The outward pointing normal vectors on the boundaries are, hence, denoted by $\boldsymbol{n}^{(i)} = \boldsymbol{\nabla} G^{(i)}/|\boldsymbol{\nabla} G^{(i)}|$. For convenience, we also define $\chi^2(x, t)$ and $\Gamma(x, t)$ to be the area of the cross-section and its total boundary length at axial position x. When the fluid passes through the aperture the velocity is $u = U_{in}$, $v = w = 0$, and we denote the area and the boundary lengths as χ_{in} and Γ_{in}, respectively. At the aperture, the shapes of the external boundary and the internal holes are denoted by $G^{(0)}_{in}(y, z) = 0$ and $G^{(i)}_{in}(y, z) = 0$, respectively.

Assuming an incompressible Newtonian fluid, the governing equations for the fluid flow are

$$\boldsymbol{\nabla} \cdot \boldsymbol{u} = 0, \tag{2.1a}$$

$$\rho \left(\frac{\partial \boldsymbol{u}}{\partial t} + \boldsymbol{u} \cdot \boldsymbol{\nabla} \boldsymbol{u} \right) = -\boldsymbol{\nabla} p + \boldsymbol{\nabla} \cdot \boldsymbol{\sigma}, \tag{2.1b}$$

where ρ is the density of the fluid, $\boldsymbol{\sigma} = \mu(\theta)(\boldsymbol{\nabla} \boldsymbol{u} + (\boldsymbol{\nabla} \boldsymbol{u})^{\mathrm{T}})$ is the usual stress tensor and $\mu(\theta)$ is the viscosity of the fluid.

On the external surface of the cylinder and on the N internal surfaces, the dynamic and kinematic boundary conditions are

$$\boldsymbol{\sigma} \cdot \boldsymbol{n}^{(i)} = -\gamma(\theta)\kappa^{(i)}\boldsymbol{n}^{(i)} + \boldsymbol{\nabla}^{(i)}_S \gamma(\theta), \quad i = 0, 1, \ldots, N, \tag{2.1c}$$

$$\frac{\partial G^{(i)}}{\partial t} + \boldsymbol{u} \cdot \boldsymbol{\nabla} G^{(i)} = 0, \quad i = 0, 1, \ldots, N, \tag{2.1d}$$

where $\gamma(\theta)$ is the surface-tension coefficient, $\kappa^{(i)}$ is the local curvature of the ith boundary, and $\boldsymbol{\nabla}_S^{(i)} = \boldsymbol{\nabla} - \boldsymbol{n}^{(i)}\partial/\partial\boldsymbol{n}^{(i)}$ is the surface gradient on the ith boundary. At the exit of the device the speed of the (now solid) thread is controlled by the take-up roller and hence given by $u = U_{out}$ and $v = w = 0$ at $x = L$.

The governing equation for the temperature θ is given by

$$\rho c_p \left(\frac{\partial \theta}{\partial t} + \boldsymbol{u} \cdot \boldsymbol{\nabla}\theta \right) = k\nabla^2\theta, \tag{2.2a}$$

where c_p and k are the specific heat and conductivity of the glass, respectively. Here we have neglected the effects of radiative heat penetrating into the interior of the glass. This is because the glass can be approximated as being optically thick for wavelengths that dominate the radiative heat transfer (Modest 2013). Radiative heating is therefore assumed to occur only at the external boundary of the thread. At the external boundary, the thread is also cooled by blowing cold gas through the device. Hence we have the boundary condition

$$-k\boldsymbol{\nabla}\theta \cdot \boldsymbol{n}^{(0)} = F_R(\theta) + F_C(\theta), \quad \text{on } G^{(0)}(\boldsymbol{x}, t) = 0, \tag{2.2b}$$

where $F_R(\theta)$ and $F_C(\theta)$ are the radiative and convective heat transfer rates, respectively. We will assume that F_R is given by

$$F_R(\theta, x) = \begin{cases} k_b\beta(\theta^4 - \theta_h^4(x)), & 0 \leqslant x \leqslant L_h, \\ k_b\beta(\theta^4 - \theta_a^4), & L_h < x \leqslant L, \end{cases} \tag{2.2c}$$

where k_b is the Stefan–Boltzmann constant, β is the absorptivity of the glass surface, θ_a is the ambient temperature and $\theta_h(x)$ is the effective temperature of the heater that, in general, will be spatially dependent. We will further assume that F_C is given by

$$F_C(\theta) = h_w(\theta - \theta_a), \tag{2.2d}$$

where h_w is the heat transfer coefficient for convective gas flow and the temperature of the gas is assumed to be the same as the ambient temperature. In writing down (2.2c), we have assumed that the ambient temperature is a constant. We will assume that radiative heat transfer across internal cavities will be negligible compared to the heat transfer from the external boundary and, thus, we assume that

$$-k\boldsymbol{\nabla}\theta \cdot \boldsymbol{n}^{(i)} = 0, \quad \text{on } G^{(i)}(\boldsymbol{x}, t) = 0, \, i \neq 0. \tag{2.2e}$$

This assumption is reasonable in the case that there is no significant cooling arising from any gas flow through the internal cavities (which is here assumed to be negligible). At the aperture the temperature is specified,

$$\theta = \theta_{in}, \quad \text{at } x = 0. \tag{2.2f}$$

In principle, we also need to specify a boundary condition on the temperature at the take-up roller. The exact details of this condition will depend on the nature of the take-up roller. We will later show that the axial conduction terms are small and that for our purposes such a condition is not required.

The theory we will develop will be appropriate for arbitrary viscosity–temperature and surface tension–temperature relations. However, for definiteness, we will use the

following empirical relations that have been widely used in the literature. We will assume that the viscosity–temperature relation is given by the Vogel–Fulcher–Tamann (VFT) equation (Scherer 1992) with parameters obtained by empirically fitting using the data for F2 glass (K. Richardson, 2012, private communication as part of NSF-DMR #0807016 'Materials world network in advanced optical glasses for novel optical fibers'),

$$\log_{10}\mu = -2.314 + \frac{4065.2}{\theta - 410.15}, \tag{2.3}$$

where the temperature θ is measured in Kelvin and μ is given in Pa s. The relation between the surface-tension coefficient of F2 glass and temperature can be fitted using the data in Boyd *et al.* (2012) to give

$$\gamma = 0.23(1 - 2\times 10^{-4}(\theta - 1373)), \tag{2.4}$$

where the surface tension is measured in N m^{-1}. This magnitude of variation is also broadly consistent with the data of Shartsis & Spinner (1951) for a wide range of silica glasses.

2.2. *Scaling and slenderness approximation for the steady state problem*

There are some subtleties that one must take into account when choosing scales for non-dimensionalisation. In particular, when selecting a scale for the viscosity, we are faced with the issue that the viscosity of the glass varies by many orders of magnitude as the temperature changes. In order to select an appropriate scale, one should select a viscosity at which the majority of the deformation occurs. This is clearly not the input temperature at which the viscosity is extremely high. However, it is also not the viscosity associated with the temperature of the radiative heater because the convective cooling means that the maximum temperature the thread can attain is significantly lower than the radiative heater temperature. Therefore, a useful quantity is the temperature at which heating from the radiative source (at the location with the strongest heating) balances the convective cooling. We denote this temperature as θ_{hot} which, from (2.2*b*), is given by solving the equation

$$k_b\beta(\theta_{hot}^4 - \max_x\{\theta_h^4(x)\}) + h_w(\theta_{hot} - \theta_a) = 0. \tag{2.5}$$

Thus, θ_{hot} represents the maximum temperature that the glass would achieve if it were placed in the heater and allowed to reach equilibrium. We then use this value of the temperature to define $\mu_{hot} = \mu(\theta_{hot})$ which we will choose as our viscosity scale. Table 1 shows typical parameter values for fibre drawing assuming the preform material is F2 glass, a commercial lead-silicate glass from the Schott Glass Company whose physical properties are provided in the company's Optical Glass – Collection Data Sheets (https://www.schott.com/advanced_optics/english/download/index.html). Other parameter values are consistent with experiments performed in the Institute for Photonics and Advanced Sensing (IPAS) at The University of Adelaide. Using these values and solving the above quartic equation we obtain $\theta_{hot} \approx 1020$ K and $\mu_{hot} \approx 2\times 10^4$ Pa s. This means that the viscosity varies by approximately 10 orders of magnitude over $\theta_{in} \leqslant \theta \leqslant \theta_{hot}$. Although the variation of surface tension with temperature is much less dramatic (typically approximately 5–10 %), it can

Parameter	Symbol	Approx. value	Units
Surface absorptivity/emissivity	β	0.8	—
Surface tension at temperature θ_{hot}	γ_{hot}	0.24	N m^{-1}
Ambient air temperature	θ_a	290	K
Input glass temperature	θ_{in}	650	K
Equilibrium temperature	θ_{hot}	970	K
Maximum heater temperature	$\max_x\{\theta_h(x)\}$	1230	K
Viscosity at temperature θ_{hot}	μ_{hot}	2×10^4	Pa s
Density	ρ	3600	kg m^{-3}
Preform cross-sectional area	χ_{in}^2	10^{-4}	m^2
Specific heat	c_p	557	J kg^{-1} K^{-1}
Draw ratio	D	10^3–10^4	—
Heat transfer coefficient	h_w	95	W m^{-2} K^{-1}
Conductivity	k	0.78	W m^{-1} K^{-1}
Stefan–Boltzmann constant	k_b	5.67×10^{-8}	W m^{-2} K^{-4}
Neck-down length	L	0.2	m
Heater length	L_h	0.05	m
Feed speed	U_{in}	2.3×10^{-5}	m s^{-1}

TABLE 1. Typical parameters for drawing a fibre from a preform made from F2 glass.

still be significant in affecting the evolution of the shape of the thread. We choose $\gamma_{hot} = \gamma(\theta_{hot}) \approx 0.24$ N m^{-1} as a typical scale for the surface tension.

Moreover, draw towers tend to be a few metres in length, but for the vast majority of this length, the thread will be sufficiently cool that the viscosity will be much too high for any meaningful deformation to occur. We therefore choose the axial length scale to be a length beyond which no significant deformation occurs and denote this as L. For convenience, we non-dimensionalise the radial length scales using χ_{in} that represents the square root of the cross-sectional area. With these issues in mind, we select the following scales

$$\left.\begin{gathered}(x, y, z) = L(x', \epsilon y', \epsilon z'), \quad t = \frac{L}{U_{in}} t', \quad p = \frac{\mu_{hot} U_{in}}{L} p', \\ (u, v, w) = U_{in}(u', \epsilon v', \epsilon w'), \quad \chi = \chi_{in}\chi', \quad \Gamma = \chi_{in}\Gamma', \quad \kappa = \kappa'/\chi_{in}, \\ \theta = \theta_{in} + \Theta\theta', \quad \mu(\theta) = \mu_{hot}\mu'(\theta'), \quad \gamma = \gamma_{hot}\gamma'(\theta'),\end{gathered}\right\} \tag{2.6}$$

where $\Theta = (\theta_{hot} - \theta_{in})$ and primes denote dimensionless variables.

We next consider the steady-state equations by setting $\partial_t \equiv 0$, substitute the above scalings into the governing equations and drop the primes for convenience. The momentum equation (2.1*b*) yields

$$\begin{aligned} Re\,\epsilon^2 \left(u\frac{\partial u}{\partial x} + v\frac{\partial u}{\partial y} + w\frac{\partial u}{\partial z}\right) &= -\epsilon^2 \frac{\partial p}{\partial x} \\ &+ \epsilon^2 \frac{\partial}{\partial x}\left(2\mu\frac{\partial u}{\partial x}\right) + \frac{\partial}{\partial y}\left(\mu\left[\frac{\partial u}{\partial y} + \epsilon^2\frac{\partial v}{\partial x}\right]\right) + \frac{\partial}{\partial z}\left(\mu\left[\frac{\partial u}{\partial z} + \epsilon^2\frac{\partial w}{\partial x}\right]\right), \end{aligned} \tag{2.7a}$$

$$\begin{aligned} Re\,\epsilon^2 \left(u\frac{\partial v}{\partial x} + v\frac{\partial v}{\partial y} + w\frac{\partial v}{\partial z}\right) &= -\frac{\partial p}{\partial y} \\ &+ \frac{\partial}{\partial x}\left(\mu\left[\epsilon^2\frac{\partial v}{\partial x} + \frac{\partial u}{\partial y}\right]\right) + \frac{\partial}{\partial y}\left(2\mu\frac{\partial v}{\partial y}\right) + \frac{\partial}{\partial z}\left(\mu\left[\frac{\partial v}{\partial z} + \frac{\partial w}{\partial y}\right]\right), \end{aligned} \tag{2.7b}$$

$$Re\,\epsilon^2\left(u\frac{\partial w}{\partial x}+v\frac{\partial w}{\partial y}+w\frac{\partial w}{\partial z}\right)=-\frac{\partial p}{\partial z}$$
$$+\frac{\partial}{\partial x}\left(\mu\left[\epsilon^2\frac{\partial w}{\partial x}+\frac{\partial u}{\partial z}\right]\right)+\frac{\partial}{\partial y}\left(\mu\left[\frac{\partial w}{\partial y}+\frac{\partial v}{\partial z}\right]\right)+\frac{\partial}{\partial z}\left(2\mu\frac{\partial w}{\partial z}\right), \tag{2.7c}$$

where

$$\epsilon=\frac{\chi_{in}}{L}, \tag{2.8}$$

is the slenderness parameter and

$$Re=\frac{\rho U_{in}L}{\mu_{hot}}, \tag{2.9}$$

is the Reynolds number. The continuity equation (2.1*a*) yields

$$\frac{\partial u}{\partial x}+\frac{\partial v}{\partial y}+\frac{\partial w}{\partial z}=0. \tag{2.10}$$

The boundary conditions (2.1*c*) are given by

$$\epsilon^2\left(-p+2\mu\frac{\partial u}{\partial x}\right)n_x^{(i)}+\mu\left(\frac{\partial u}{\partial y}+\epsilon^2\frac{\partial v}{\partial x}\right)n_y^{(i)}+\mu\left(\frac{\partial u}{\partial z}+\epsilon^2\frac{\partial w}{\partial x}\right)n_z^{(i)}$$
$$=\frac{\epsilon^2}{Ca}\left(-\gamma\kappa^{(i)}n_x^{(i)}+\frac{\partial\gamma}{\partial x}-\left[\epsilon^2\frac{\partial\gamma}{\partial x}n_x^{(i)}+\frac{\partial\gamma}{\partial y}n_y^{(i)}+\frac{\partial\gamma}{\partial z}n_z^{(i)}\right]n_x^{(i)}\right), \tag{2.11a}$$
$$\left(-p+2\mu\frac{\partial v}{\partial y}\right)n_y^{(i)}+\mu\left(\epsilon^2\frac{\partial v}{\partial x}+\frac{\partial u}{\partial y}\right)n_x^{(i)}+\mu\left(\frac{\partial v}{\partial z}+\frac{\partial w}{\partial y}\right)n_z^{(i)}$$
$$=\frac{1}{Ca}\left(-\gamma\kappa^{(i)}n_y^{(i)}+\frac{\partial\gamma}{\partial y}-\left[\epsilon^2\frac{\partial\gamma}{\partial x}n_x^{(i)}+\frac{\partial\gamma}{\partial y}n_y^{(i)}+\frac{\partial\gamma}{\partial z}n_z^{(i)}\right]n_y^{(i)}\right), \tag{2.11b}$$
$$\left(-p+2\mu\frac{\partial w}{\partial z}\right)n_z^{(i)}+\mu\left(\epsilon^2\frac{\partial w}{\partial x}+\frac{\partial u}{\partial z}\right)n_x^{(i)}+\mu\left(\frac{\partial v}{\partial z}+\frac{\partial w}{\partial y}\right)n_y^{(i)}$$
$$=\frac{1}{Ca}\left(-\gamma\kappa^{(i)}n_z^{(i)}+\frac{\partial\gamma}{\partial z}-\left[\epsilon^2\frac{\partial\gamma}{\partial x}n_x^{(i)}+\frac{\partial\gamma}{\partial y}n_y^{(i)}+\frac{\partial\gamma}{\partial z}n_z^{(i)}\right]n_z^{(i)}\right), \tag{2.11c}$$

where

$$Ca=\frac{\mu_{hot}U_{in}\chi_{in}}{\gamma_{hot}L}, \tag{2.12}$$

is the effective capillary number and it is understood that γ is a function of $\theta(x,y,z)$. Note that the constant dimensionless surface-tension parameter γ^* defined in Stokes *et al.* (2014) is a function of θ for temperature-dependent surface tension, and

$$\gamma^*(\theta)\equiv\frac{\gamma(\theta)}{Ca}, \tag{2.13}$$

in the notation of this paper. The steady-state kinematic conditions (2.1*d*) are invariant under the scaling and are hence given by

$$u\frac{\partial G^{(i)}}{\partial x}+v\frac{\partial G^{(i)}}{\partial y}+w\frac{\partial G^{(i)}}{\partial z}=0. \tag{2.14}$$

The boundary conditions at the aperture $x = 0$ are given by

$$u = 1, \quad v = w = 0, \quad \text{and} \quad \chi = 1, \tag{2.15a–c}$$

whereas the boundary conditions at the take-up roller and, hence, at $x = 1$, are given by

$$u = D, \quad v = w = 0, \tag{2.16a,b}$$

where

$$D = \frac{U_{out}}{U_{in}}, \tag{2.17}$$

is the draw ratio.

The steady-state energy conservation equation (2.2*a*) takes the form

$$\epsilon^2 Pe \left(u\frac{\partial \theta}{\partial x} + v\frac{\partial \theta}{\partial y} + w\frac{\partial \theta}{\partial z} \right) = \epsilon^2 \frac{\partial^2 \theta}{\partial x^2} + \frac{\partial^2 \theta}{\partial y^2} + \frac{\partial^2 \theta}{\partial z^2}, \tag{2.18}$$

where

$$Pe = \frac{\rho c_p U_{in} L}{k}, \tag{2.19}$$

is the Péclet number. The boundary condition on the external surface of the thread (2.2*b*) becomes

$$-\left(\epsilon^2 \frac{\partial \theta}{\partial x} n_x^{(0)} + \boldsymbol{\nabla}_\perp \theta \cdot \boldsymbol{n}_\perp^{(0)} \right) = \frac{\epsilon^2 Pe}{Ca} [\mathcal{H}_R f_R(\theta, x) + \mathcal{H}_C f_C(\theta)], \tag{2.20}$$

where

$$\mathcal{H}_R = \frac{\beta k_b \theta_{hot}^4 \mu_{hot}}{\rho c_p \Theta \gamma_{hot}}, \quad \text{and} \quad \mathcal{H}_C = \frac{h_w \theta_{hot} \mu_{hot}}{\rho c_p \Theta \gamma_{hot}}, \tag{2.21a,b}$$

are the dimensionless parameters that represent the importance of radiative and convective cooling, respectively. Here, $\boldsymbol{\nabla}_\perp = (\partial/\partial y, \partial/\partial z)$, $\boldsymbol{n}_\perp^{(i)} = (n_y^{(i)}, n_z^{(i)})$,

$$f_C(\theta) = (1 - \vartheta_{in})\theta + \vartheta_{in} - \vartheta_a, \tag{2.22a}$$

and

$$f_R(\theta, x) = \begin{cases} (\theta + \vartheta_{in}(1-\theta))^4 - (\vartheta_h(x))^4, & 0 \leqslant x \leqslant \ell, \\ (\theta + \vartheta_{in}(1-\theta))^4 - \vartheta_a^4, & \ell < x \leqslant 1, \end{cases} \tag{2.22b}$$

where

$$\vartheta_{in} = \frac{\theta_{in}}{\theta_{hot}}, \quad \vartheta_a = \frac{\theta_a}{\theta_{hot}}, \quad \text{and} \quad \vartheta_h(x) = \frac{\theta_h(x)}{\theta_{hot}}, \tag{2.22c–e}$$

are the input glass, ambient air and heater temperatures scaled with θ_{hot}, and

$$\ell = L_h/L, \tag{2.22f}$$

is the dimensionless length of the heater. On internal air-channel surfaces the boundary condition (2.2*e*) is given by

$$-\left(\epsilon^2\frac{\partial\theta}{\partial x}n_x^{(i)}+\boldsymbol{\nabla}_\perp\theta\cdot\boldsymbol{n}_\perp^{(i)}\right)=0. \tag{2.23}$$

From the typical parameter values for fibre drawing given in table 1, we see that $\epsilon = O(10^{-1})$. As is typical in the modelling of fibre drawing problems (Yarin *et al.* 1989; Dewynne *et al.* 1994; Cummings & Howell 1999; Stokes *et al.* 2000, 2014; Fitt *et al.* 2002; Wylie *et al.* 2007; Griffiths & Howell 2008; Taroni *et al.* 2013), we exploit the fact that $\epsilon \ll 1$ to develop long-wavelength equations that are significantly simpler to deal with than the full equations given above. Thus, we expand all dependent variables in powers of ϵ^2,

$$\left.\begin{aligned}\theta &= \theta_0(x,y,z)+\epsilon^2\theta_1(x,y,z)+\epsilon^4\theta_2(x,y,z)+\cdots,\\ u &= u_0(x,y,z)+\epsilon^2u_1(x,y,z)+\epsilon^4u_2(x,y,z)+\cdots,\end{aligned}\right\} \tag{2.24}$$

and similarly for v, w, p, $G^{(i)}$, $\kappa^{(i)}$, χ and $\Gamma^{(i)}$. These expressions are then substituted into (2.7), (2.10), (2.11), (2.14)–(2.16), (2.18), (2.20), (2.22) and (2.23). Assuming $\epsilon^2 Pe \ll 1$, at leading order we obtain

$$\nabla_\perp^2\theta_0 = 0, \tag{2.25a}$$

$$\boldsymbol{\nabla}_\perp\theta_0\cdot\boldsymbol{n}_\perp^{(i)} = 0, \quad \text{on all boundaries } i=0,1,\ldots,N, \tag{2.25b}$$

where $\nabla_\perp^2$ is the two-dimensional Laplacian in the y–z plane. From this we deduce that $\theta_0 = \theta_0(x)$, i.e. the leading-order temperature is independent of the cross-plane position. Therefore, the viscosity and surface tension (that are functions of temperature only) are, at leading order, also independent of the cross-plane position. With the additional assumption $\epsilon^2 Re \ll 1$, the leading-order momentum equation and boundary conditions are then

$$\nabla_\perp^2 u_0 = 0, \tag{2.26a}$$

$$\boldsymbol{\nabla}_\perp u_0\cdot\boldsymbol{n}_\perp^{(i)} = 0, \quad \text{for } i=0,1,\ldots,N. \tag{2.26b}$$

We hence deduce that $u_0 = u_0(x)$, that is the leading-order axial velocity is also independent of the cross-plane position. Thus, we have established that the leading-order temperature θ_0, axial velocity u_0, viscosity $\mu(\theta_0)$ and surface tension $\gamma(\theta_0)$ are all independent of y and z and, so, functions of x only.

2.3. *Leading-order axial-flow model*

We obtain our leading-order axial-flow model by considering $O(\epsilon^2)$ terms from the axial-flow equation, to give

$$\begin{aligned}\boldsymbol{\nabla}_\perp\cdot(\mu_0\boldsymbol{\nabla}_\perp u_1) \;=\; & Re\,u_0\frac{\partial u_0}{\partial x}+\frac{\partial p_0}{\partial x}-\frac{\partial}{\partial x}\left(2\mu(\theta_0)\frac{\partial u_0}{\partial x}\right)\\ & -\frac{\partial}{\partial y}\left(\mu(\theta_0)\frac{\partial v_0}{\partial x}\right)-\frac{\partial}{\partial z}\left(\mu(\theta_0)\frac{\partial w_0}{\partial x}\right),\end{aligned} \tag{2.27a}$$

with boundary conditions

$$\mu(\theta_0)\nabla_\perp u_1 = -\mu(\theta_0)\left(\frac{\partial v_0}{\partial x}n_y^{(i)} + \frac{\partial w_0}{\partial x}n_z^{(i)}\right) + \left(p_0 - 2\mu(\theta_0)\frac{\partial u_0}{\partial x}\right)n_x^{(i)} + \frac{1}{Ca}\left(-\gamma(\theta_0)\kappa_0^{(i)}n_x^{(i)} + \frac{\partial}{\partial x}(\gamma(\theta_0))\right). \tag{2.27b}$$

Following a procedure developed by Dewynne *et al.* (1994) and Cummings & Howell (1999), equation (2.27*a*) and the boundary condition (2.27*b*) are effectively integrated over the cross-sectional area to obtain the axial force balance equation

$$-Re\,\chi_0^2 u_0\frac{\partial u_0}{\partial x} + \frac{\partial}{\partial x}\left(3\mu(\theta_0)\chi_0^2\frac{\partial u_0}{\partial x}\right) + \frac{1}{2Ca}\frac{\partial}{\partial x}(\gamma(\theta_0)\Gamma_0) = 0. \tag{2.28}$$

Similarly, the continuity equation (2.10) and the steady-state kinematic condition (2.34*e*) are effectively integrated over the cross-sectional area to obtain

$$\frac{\partial}{\partial x}(u_0\chi_0^2) = 0, \tag{2.29}$$

which, on integrating again and applying the boundary conditions (2.15), yields the continuity equation

$$u_0\chi_0^2 = 1. \tag{2.30}$$

Substituting (2.30) in the first term in (2.28) we see that (2.28) may be integrated after which, using (2.30) to substitute for u_0, we obtain

$$-Re\frac{1}{\chi_0^2} - 3\mu(\theta_0)\frac{1}{\chi_0^2}\frac{\partial\chi_0^2}{\partial x} + \frac{1}{2Ca}\gamma(\theta_0)\Gamma_0 = 6T, \tag{2.31}$$

where $6T$ is the constant (dimensionless) tension in the fibre.

In general, the leading-order total boundary length of the cross-section at x, $\Gamma_0(x)$, must be obtained by solving for the flow in the cross-section. We will come to this after obtaining the leading-order temperature model.

2.4. *Leading-order temperature model*

The leading-order temperature model is obtained by taking $O(\epsilon^2)$ terms from (2.18) to give

$$Pe\,u_0\frac{\partial\theta_0}{\partial x} = \frac{\partial^2\theta_0}{\partial x^2} + \frac{\partial^2\theta_1}{\partial y^2} + \frac{\partial^2\theta_1}{\partial z^2}, \tag{2.32a}$$

along with boundary conditions

$$-\left(\frac{\partial\theta_0}{\partial x}n_x^{(0)} + \nabla_\perp\theta_1\cdot\boldsymbol{n}_\perp^{(0)}\right) = \frac{Pe}{Ca}[\mathcal{H}_R f_R(\theta_0, x) + \mathcal{H}_C f_C(\theta_0)], \tag{2.32b}$$

on the external boundary $G_0^{(0)}(\boldsymbol{x}) = 0$ and

$$\frac{\partial\theta_0}{\partial x}n_x^{(i)} + \nabla_\perp\theta_1\cdot\boldsymbol{n}_\perp^{(i)} = 0, \tag{2.32c}$$

on internal boundaries $G_0^{(i)}(\boldsymbol{x}) = 0$, $i \neq 0$.

Integrating (2.32*a*) over the cross-sectional area and using (2.32*b*) and (2.32*c*) yields

$$u_0\frac{\partial\theta_0}{\partial x}=\frac{1}{Pe\chi_0^2}\frac{\partial}{\partial x}\left(\chi_0^2\frac{\partial\theta_0}{\partial x}\right)-\frac{\Gamma_0^{(0)}}{Ca\chi_0^2}[\mathcal{H}_R f_R(\theta_0,x)+\mathcal{H}_C f_C(\theta_0)], \tag{2.33}$$

where $\Gamma_0^{(0)}$ is the leading-order length of the external boundary which also must, in general, be found by solving for the flow in the cross-section.

2.5. *Leading-order transverse-flow model*

The equations for the flow in the cross-section are obtained by taking the leading-order terms from the transverse-flow equations, and are given by

$$-\frac{\partial p_0}{\partial y}+\frac{\partial}{\partial y}\left(2\mu(\theta_0)\frac{\partial v_0}{\partial y}\right)+\frac{\partial}{\partial z}\left(\mu(\theta_0)\left[\frac{\partial v_0}{\partial z}+\frac{\partial w_0}{\partial y}\right]\right)=0, \tag{2.34a}$$

$$-\frac{\partial p_0}{\partial z}+\frac{\partial}{\partial y}\left(\mu(\theta_0)\left[\frac{\partial w_0}{\partial y}+\frac{\partial v_0}{\partial z}\right]\right)+\frac{\partial}{\partial z}\left(2\mu(\theta_0)\frac{\partial w_0}{\partial z}\right)=0, \tag{2.34b}$$

with boundary conditions

$$\left(-p_0+2\mu(\theta_0)\frac{\partial v_0}{\partial y}\right)n_y^{(i)}+\mu(\theta_0)\left(\frac{\partial v_0}{\partial z}+\frac{\partial w_0}{\partial y}\right)n_z^{(i)}=\frac{1}{Ca}(-\gamma(\theta_0)\kappa_0^{(i)}n_y^{(i)}), \tag{2.34c}$$

$$\left(-p_0+2\mu(\theta_0)\frac{\partial w_0}{\partial z}\right)n_z^{(i)}+\mu(\theta_0)\left(\frac{\partial v_0}{\partial z}+\frac{\partial w_0}{\partial y}\right)n_y^{(i)}=\frac{1}{Ca}(-\gamma(\theta_0)\kappa_0^{(i)}n_z^{(i)}), \tag{2.34d}$$

$$u_0\frac{\partial G_0^{(i)}}{\partial x}+v_0\frac{\partial G_0^{(i)}}{\partial y}+w_0\frac{\partial G_0^{(i)}}{\partial z}=0, \tag{2.34e}$$

for $i=0,\ldots,N$. In addition we must satisfy the continuity condition

$$\frac{\partial v_0}{\partial y}+\frac{\partial w_0}{\partial z}=-\frac{\partial u_0}{\partial x}. \tag{2.35}$$

As done by Dewynne *et al.* (1994), Cummings & Howell (1999) and Stokes *et al.* (2014), but with a modification to take into account temperature-dependent surface tension and viscosity, we write the flow in the cross-section as the sum of the solution in the absence of surface tension and a component due to the surface tension, namely,

$$p_0=-\mu(\theta_0)\frac{\partial u_0}{\partial x}+\frac{1}{Ca}\frac{\gamma(\theta_0)}{\chi}\tilde{p},\quad (v_0,w_0)=-\frac{1}{2}\frac{\partial u_0}{\partial x}(y,z)+\frac{1}{Ca}\frac{\gamma(\theta_0)}{\mu(\theta_0)}(\tilde{v},\tilde{w}). \tag{2.36a,b}$$

Here, $\tilde{p}$, $\tilde{v}$ and $\tilde{w}$ represent the scaled deformation due to surface tension. The scalings $\gamma/(Ca\chi)$ and $\gamma/(Ca\mu)$ in (2.36) are selected to simplify the resulting cross-plane flow problem. Note that the solution for constant viscosity ($\mu=1$) and zero surface tension ($1/Ca=0$) was first obtained by Dewynne *et al.* (1992). We next replace the variable x by the reduced time τ, introduced by Cummings & Howell (1999) for constant viscosity and surface tension, but here defined for viscosity and surface tension that both depend on temperature by

$$\frac{\mathrm{d}\tau}{\mathrm{d}x}=\frac{\gamma(\theta_0)\chi_0}{Ca\,\mu(\theta_0)},\quad \text{with } \tau=0 \text{ at } x=0. \tag{2.37}$$

We also scale the transverse coordinates and boundary lengths with $\chi_0(\tau)$ so that

$$(y, z) = \chi_0(\tilde{y}, \tilde{z}), \quad \Gamma^{(i)} = \chi_0 \tilde{\Gamma}^{(i)}, \quad \tilde{\kappa} = \chi_0 \kappa. \tag{2.38a–c}$$

Using these transformations and subtracting the zero-surface-tension eigensolution we obtain

$$\tilde{v}_{\tilde{y}} + \tilde{w}_{\tilde{z}} = 0, \tag{2.39a}$$

$$\tilde{v}_{\tilde{y}\tilde{y}} + \tilde{v}_{\tilde{z}\tilde{z}} = \tilde{p}_{\tilde{y}}, \tag{2.39b}$$

$$\tilde{w}_{\tilde{y}\tilde{y}} + \tilde{w}_{\tilde{z}\tilde{z}} = \tilde{p}_{\tilde{z}}, \tag{2.39c}$$

$$G^{(i)}_{\tau} + \tilde{v} G^{(i)}_{\tilde{y}} + \tilde{w} G^{(i)}_{\tilde{z}} = 0, \quad \text{on } G^{(i)}(\tau, \tilde{y}, \tilde{z}) = 0, \tag{2.39d}$$

$$G^{(i)}_{\tilde{y}}(-\tilde{p} + 2\tilde{v}_{\tilde{y}}) + G^{(i)}_{\tilde{z}}(\tilde{v}_{\tilde{z}} + \tilde{w}_{\tilde{y}}) = -\tilde{\kappa} G^{(i)}_{\tilde{y}}, \quad \text{on } G^{(i)}(\tau, \tilde{y}, \tilde{z}) = 0, \tag{2.39e}$$

$$G^{(i)}_{\tilde{y}}(\tilde{v}_{\tilde{z}} + \tilde{w}_{\tilde{y}}) + G^{(i)}_{\tilde{z}}(-\tilde{p} + 2\tilde{w}_{\tilde{z}}) = -\tilde{\kappa} G^{(i)}_{\tilde{z}}, \quad \text{on } G^{(i)}(\tau, \tilde{y}, \tilde{z}) = 0, \tag{2.39f}$$

where subscripts denote differentiation with respect to the subscript variables. These equations are the classical two-dimensional surface-tension-driven Stokes flow free boundary problem on a domain of unit area driven by unit surface tension on the boundary. We note that, using these scaled variables, the cross-sectional flow problem completely decouples from the details of the axial flow and temperature. The solution of this problem yields both the scaled total boundary length $\tilde{\Gamma}$ and the scaled outer boundary length $\tilde{\Gamma}^{(0)}$, as well as the cross-sectional geometry at each τ. One can then use (2.38) to obtain the unscaled variables $\Gamma_0 = \chi_0 \tilde{\Gamma}$ and $\Gamma_0^{(0)} = \chi_0 \tilde{\Gamma}^{(0)}$. Note too that for a circular cross-section with no holes, as for drawing a solid axisymmetric fibre, $\tilde{v} = \tilde{w} = 0$ and surface tension on the (stationary) external boundary is balanced by constant pressure, i.e. $\tilde{p} = \tilde{\kappa}$, while $\tilde{\Gamma} = 2\sqrt{\pi}$ for all (reduced) time.

2.6. *Simplified equations for the cross-sectional area and temperature*

Using the parameter estimates in table 1, we obtain

$$Re \sim 10^{-6}, \quad Pe \sim 10. \tag{2.40a,b}$$

Examining (2.30) and (2.31), we see that the largest value that the inertial term can take is at the take-up roller where it has size $ReD \sim 10^{-2}$. We will therefore neglect the inertial terms. Moreover, since $1/Pe \sim 0.1$ we will also neglect the conduction term in (2.33). Then, on using (2.37) to replace x with τ we obtain

$$\frac{\mathrm{d}\chi}{\mathrm{d}\tau} - \frac{1}{12}\tilde{\Gamma}(\tau)\chi = -\frac{Ca\ T}{\gamma(\theta)}, \quad \text{with } \chi(0) = 1 \tag{2.41}$$

and

$$\frac{\mathrm{d}\theta}{\mathrm{d}\tau} = -\frac{\mu(\theta)}{\gamma(\theta)}\tilde{\Gamma}^{(0)}[\mathcal{H}_R f_R(\theta, x(\tau)) + \mathcal{H}_C f_C(\theta)], \quad \text{with } \theta(0) = 0, \tag{2.42}$$

where, for convenience, we have dropped the subscript zeros on leading-order terms. These two ordinary differential equations (ODEs) must be solved along with the additional equation (2.37) relating x and τ, which we write as

$$\frac{\mathrm{d}x}{d\tau} = \frac{Ca\,\mu(\theta)}{\gamma(\theta)\chi}, \quad \text{with } x(0) = 0. \tag{2.43}$$

Thus, having solved the transverse-flow problem for the geometry and boundary lengths $\tilde{\Gamma}(\tau)$ and $\tilde{\Gamma}^{(0)}(\tau)$ for $\tau \geqslant 0$, we are able to solve a system of three ODEs for the cross-sectional area $\chi(\tau)$, the temperature $\theta(\tau)$ and the axial position $x(\tau)$. However, we need only compute to $x = 1$ and, therefore, stop the ODE solver when it reaches $x(\tau) = 1$ at which point $\tau = \tau_{stop}$ and the square root of the cross-sectional area of the fibre is $\chi(\tau_{stop}) = \chi_{stop}$.

There are a couple of additional matters that need comment. First, the viscosity as given by (2.3) increases without bound as the temperature decreases to 410.15 K and the solution of the ODE system fails due to numerical precision issues if the viscosity becomes too large. To overcome this problem we simply placed a very large artificial upper bound on the viscosity (sufficiently large that the fluid is essentially solid so that no significant deformation can occur). We chose this upper bound to be the viscosity at the input temperature which is typically ten orders of magnitude larger than μ_{hot}. Second, although the problem is stiff, with θ and x changing rapidly with τ beyond the heater region, this presented no difficulty in that MATLAB's ODE solvers (e.g. 'ode45') worked well for choices of the heater temperature profile $\vartheta(x)$ and fibre tension T corresponding to realistic fibre drawing. It is possible to choose parameters for which the ODE solver fails, but such parameter choices correspond to values of the fibre tension that are inappropriately large for the heater temperature and are, hence, associated with unrealistically large draw ratios ($D > 10^{20}$). Such a failure therefore indicates that a smaller value of the tension should be used or that the heater temperature should be reduced.

3. Results

3.1. *Axisymmetric tube with prescribed tension*

We first consider the simplest case of drawing an axisymmetric tube from a preform with external radius R_{in} and internal radius $\phi_{in}R_{in}$, where $0 \leqslant \phi_{in} < 1$ is the ratio of the radius of the hole to the radius of the outer surface at the point at which the thread is fed through the aperture. We begin by considering the problem that is most straightforward from a computational viewpoint, that is, a thread pulled with a fixed tension T through a heater of length ℓ with given temperature profile $\vartheta_h(x)$, $0 \leqslant x \leqslant \ell$.

The first step is to solve the evolution of the cross-sectional geometry in terms of τ using (2.39*a*)–(2.39*f*) and hence obtain the functions $\tilde{\Gamma}(\tau)$ and $\tilde{\Gamma}^{(0)}(\tau)$ required in (2.41) and (2.42). For an axisymmetric tube, this is relatively straightforward and the results were obtained by Stokes *et al.* (2014). In particular,

$$\tilde{\Gamma}(\tau) = \frac{2}{\alpha(\tau)}, \quad \text{and} \quad \tilde{\Gamma}^{(0)}(\tau) = \frac{1}{\alpha(\tau)} + \pi\alpha(\tau), \tag{3.1a,b}$$

where

$$\alpha(\tau) = \sqrt{\frac{1-\phi}{\pi\,(1+\phi)}} = \begin{cases} \dfrac{\tau}{2} + \sqrt{\dfrac{1-\phi_{in}}{\pi(1+\phi_{in})}}, & \tau < \tau_C, \\ \sqrt{\dfrac{1}{\pi}}, & \tau \geqslant \tau_C, \end{cases} \tag{3.2}$$

and τ_C in (3.2) is the value of τ at which ϕ becomes zero, i.e. the hole closes, and the (scaled) cross-section becomes a circle with unit area. This value is given by

$$\tau_C = \frac{2}{\sqrt{\pi}}\left(1 - \sqrt{\frac{1-\phi_{in}}{1+\phi_{in}}}\right). \tag{3.3}$$

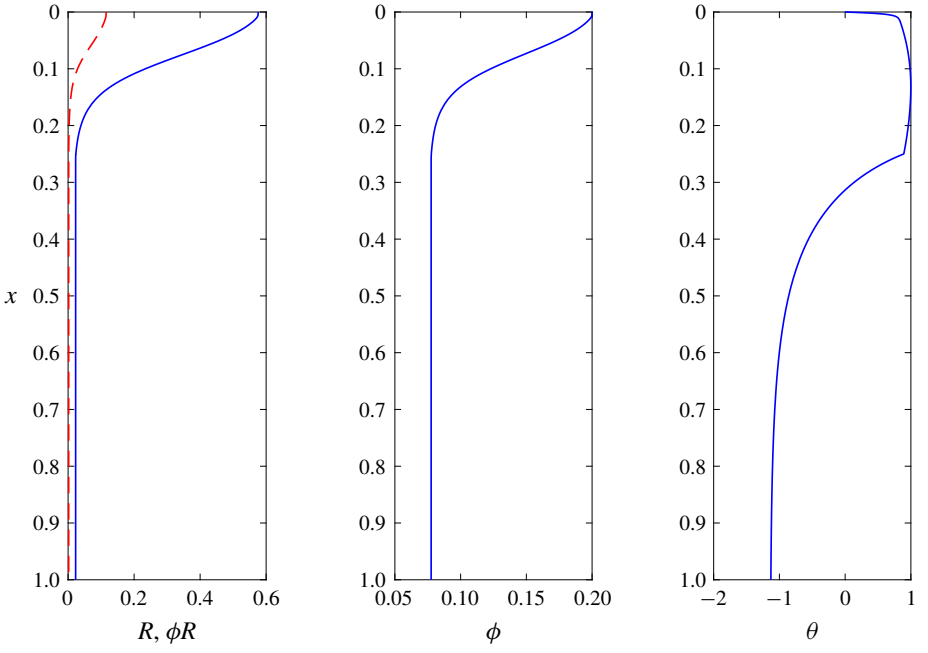

FIGURE 2. (Colour online) Solution of the forward problem for the drawing of a preform with initial aspect ratio $\phi_{in} = 0.2$ using a tension of $T = 20$ and $\vartheta(x)$ given by (3.5), yielding $\phi_{out} = 0.078$, $D = 614$ and $\chi_{out} = 0.04$. The other input parameters were $Ca = 0.40$, $\mathcal{H}_C = 57.41$, $\mathcal{H}_R = 24.74$, $\ell = 0.25$, $\vartheta_a = 0.30$ and $\vartheta_{in} = 0.67$.

Furthermore, the ratio of the radius of the hole to the radius of the outer surface at any value of τ is given by

$$\phi(\tau) = \frac{1 - \pi\alpha^2}{1 + \pi\alpha^2}. \tag{3.4}$$

Note that while a preform with $\phi_{in} > 0$ may (for a sufficiently small value of the tension T) yield a fibre with $\phi = 0$, we are not, typically, interested in such solutions since inclusion of an air channel in the preform implies that the fibre should also contain an air channel. Nevertheless, our solution method is able to handle closure of the hole.

With the functions $\tilde{\Gamma}(\tau)$ and $\tilde{\Gamma}^{(0)}(\tau)$ known, one then simply needs to numerically solve the ODE system (2.41)–(2.43) using a standard ODE solver with a stopping event at $x(\tau) = 1$. Having obtained this solution, one can reconstruct the solutions for χ, θ and ϕ as functions of x. This provides the complete solution to the problem. We note that the cross-sectional area χ^2_{stop} at $x = 1$ determines the draw ratio $D = 1/\chi^2_{stop}$ which is an output from this problem.

Figures 2 and 3 show solutions for the drawing of a preform with initial aspect ratio $\phi_{in} = 0.2$ into a fibre, with two different values of the tension T and parameters as given in the captions. The heater profile was taken to be quadratic, namely

$$\vartheta_h(x) = \frac{\theta_H - 50}{\theta_{hot}} + \frac{200}{\theta_{hot}} \frac{x(\ell - x)}{\ell^2}, \quad 0 \leqslant x \leqslant \ell, \tag{3.5}$$

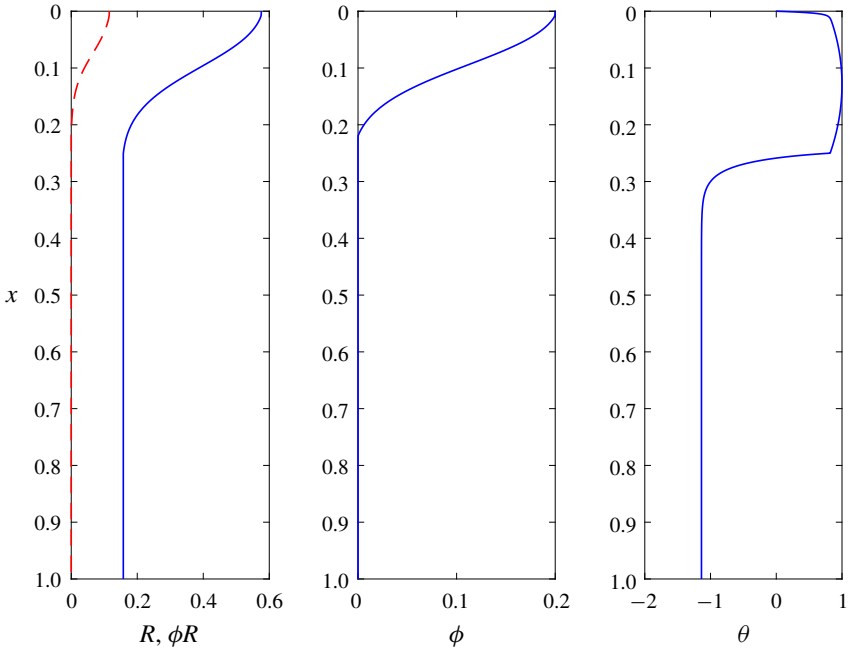

FIGURE 3. (Colour online) Solution of the forward problem for the drawing of a preform with initial aspect ratio $\phi_{in} = 0.2$ using a tension of $T = 9$ and $\vartheta(x)$ given by (3.5), yielding $\phi_{out} = 0$, $D = 12.8$ and $\chi_{out} = 0.28$. The other input parameters were $Ca = 0.40$, $\mathcal{H}_C = 57.41$, $\mathcal{H}_R = 24.74$, $\ell = 0.25$, $\vartheta_a = 0.30$ and $\vartheta_{in} = 0.67$.

with $\theta_H = \max_x\{\theta_h(x)\} = 1230$ K and $\theta_{hot} = 966.4$ K as given by solution of (2.5). The first is a case for which $\phi_{out} > 0$ while the second is a case for which the channel closes so that $\phi_{out} = 0$.

3.2. *Axisymmetric tube with prescribed draw ratio*

A situation more frequently encountered in experiments is that in which the draw ratio D (equivalently the pulling speed) is specified at the exit, but the tension T is unknown. This problem is readily solved by adapting the code for solving the problem of § 3.1 to a function having the tension T as an input parameter. Noting that the cross-sectional area at $x = 1$ must be $\chi_{out}^2 = 1/D$, a standard root-finding procedure (for example 'fzero' in MATLAB) may be used, together with an interval in which one expects to find the value T, to find the solution that satisfies $\chi_{stop} - \chi_{out} = 0$.

We note that during the root-finding procedure it is possible for the ODE solver to fail if the search interval for T contains unrealistically large values of T for the chosen maximum heater temperature θ_H. This is due to the stiffness of the problem as discussed at the end of § 2. However, it is straightforward to make our root-finding procedure robust against such failures simply by taking the effective value of χ_{stop} as the last value computed by the ODE solver before it fails (corresponding to an $x < 1$) and then using this value to evaluate $\chi_{stop} - \chi_{out}$. In general, and for all the cases we tried, the root-finding procedure continues without difficulty until the correct value of T is found.

Figure 4 shows the solution for the drawing of a preform with initial aspect ratio $\phi_{in} = 0.2$ into a fibre, with a draw ratio $D = 5000$ ($\chi = 0.014$) and other

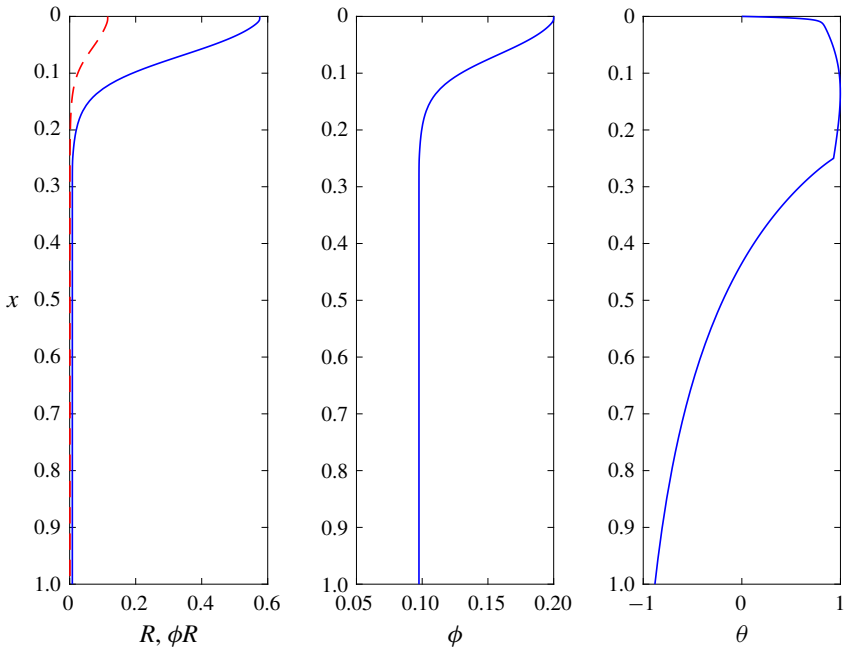

FIGURE 4. (Colour online) Solution of the forward problem for the drawing of a preform with initial aspect ratio $\phi_{in} = 0.2$ using a draw ratio of $D = 5000$ ($\chi_{out} = 0.014$) and $\vartheta(x)$ given by (3.5), yielding $\phi_{out} = 0.098$ and $T = 24.63$. The other input parameters were $Ca = 0.40$, $\mathcal{H}_C = 57.41$, $\mathcal{H}_R = 24.74$, $\ell = 0.25$, $\vartheta_a = 0.30$ and $\vartheta_{in} = 0.67$.

input parameters as used previously. The tension value found for this problem was $T = 24.6321$ (6 significant figures) while $\phi_{out} = 0.098$. Substituting this value of T into the code of § 3.1, which uses a prescribed tension, yields $D = 5000.1$ and $\phi_{out} = 0.098$, which confirms the accuracy of our method.

3.3. *Inverse problem for an axisymmetric tube*

We now consider the most practically important case in which both the inner and outer radii of the thread at both the aperture and the exit are prescribed. We shall explicitly exclude closure of any air channel during the drawing process since the sensible choice of preform for such a fibre is one without the air channel. Thus, this is a very typical case in which the preform has already been manufactured, and the parameters for the draw tower must be selected to obtain a desired final shape. Since the cross-sectional areas at the aperture and exit are prescribed, we can use (2.16) and (2.30) to obtain the draw ratio D.

For a preform that is an axisymmetric tube, the aspect ratio of the annular cross-section reduces under surface tension from aperture to exit, and the values at the aperture and the exit allow us to use (3.2) to compute the required value of τ at $x = 1$ which we denote τ_{out}. This is given by

$$\tau_{out} = 2\sqrt{\frac{1-\phi_{out}}{\pi(1+\phi_{out})}} - 2\sqrt{\frac{1-\phi_{in}}{\pi(1+\phi_{in})}}, \tag{3.6}$$

where ϕ_{out} is the ratio of the radius of the hole to the radius of the outer surface at the exit and ϕ_{in} is the same ratio at the inlet, as has been previously defined.

In § 3.1 we completely specified $\vartheta_h(x)$ and T and determined $\tau_{out} \equiv \tau_{stop}$ and D, while in § 3.2 we specified $\vartheta_h(x)$ and D and determined $\tau_{out} \equiv \tau_{stop}$ and T. Now we wish to specify τ_{out} and D and determine $\vartheta_h(x)$, and T. This is a more challenging task and a unique choice of the heater profile $\vartheta_h(x)$ cannot be expected, a matter that we will return to at the end of this section. For now, we shall suppose that the heater temperature $\vartheta_h(x)$ is parameterised by a single dimensional parameter $\theta_H = \max_x\{\theta_h(x)\}$ which also gives θ_{hot} using (2.5).

Now, the solution of (2.41) may be written exactly as

$$\chi(\tau) = \frac{1}{H(\tau)}\left(1 - Ca\,T\int_0^{\tau}\frac{H(\tau')}{\gamma(\theta(\tau'))}\,\mathrm{d}\tau'\right), \tag{3.7}$$

in terms of the integrating factor

$$H(\tau) = \exp\left(-\frac{1}{12}\int_0^{\tau}\tilde{\Gamma}(\tau')\,\mathrm{d}\tau'\right), \tag{3.8}$$

which for axisymmetric tubes is given by

$$H(\tau) = \begin{cases} \left(\dfrac{\tau}{2\alpha_{in}} + 1\right)^{-1/3}, & \tau \leqslant \tau_C, \\ \left(\dfrac{\tau_C}{2\alpha_{in}} + 1\right)^{-1/3} \exp\left(-\dfrac{\sqrt{\pi}}{6}(\tau - \tau_C)\right), & \tau > \tau_C, \end{cases} \tag{3.9}$$

where $\alpha_{in} = \alpha(0)$ as given by (3.2) and τ_C is given by (3.3). We may now set $\tau = \tau_{out}$ in (3.7) and use the fact that $\chi(\tau_{out}) = 1/\sqrt{D}$, to obtain

$$\frac{1}{\sqrt{D}} = \frac{1}{H(\tau_{out})}\left(1 - Ca\,T\int_0^{\tau_{out}}\frac{H(\tau)}{\gamma(\theta(\tau))}\,\mathrm{d}\tau\right), \tag{3.10}$$

which, if the surface tension is assumed to be independent of temperature, becomes a temperature-independent expression relating D, τ_{out} and T. Rearranging gives an explicit expression for the fibre tension T in terms of the draw ratio D and τ_{out},

$$T = \left(1 - \frac{H(\tau_{out})}{\sqrt{D}}\right)\left(\frac{Ca}{\gamma}\int_0^{\tau_{out}} H(\tau)\,\mathrm{d}\tau\right)^{-1}. \tag{3.11}$$

Note that for an axisymmetric tube with $H(\tau)$ given by (3.9), one can obtain an exact expression for the integral in (3.10) and (3.11), using the fact that $\tau_{out} < \tau_C$, namely,

$$\int_0^{\tau_{out}} H(\tau)\,\mathrm{d}\tau = 3\alpha_{in}\left[\left(\frac{\tau_{out}}{2\alpha_{in}} + 1\right)^{2/3} - 1\right]. \tag{3.12}$$

We also note that the value of the tension T that we obtain may not always be physically realistic. This is because it may be sufficiently large that the breaking stress of the fibre is exceeded or sufficiently small that the fibre cannot be drawn because the viscosity of the fibre material is too low. However, this does not prevent us from finding the solution.

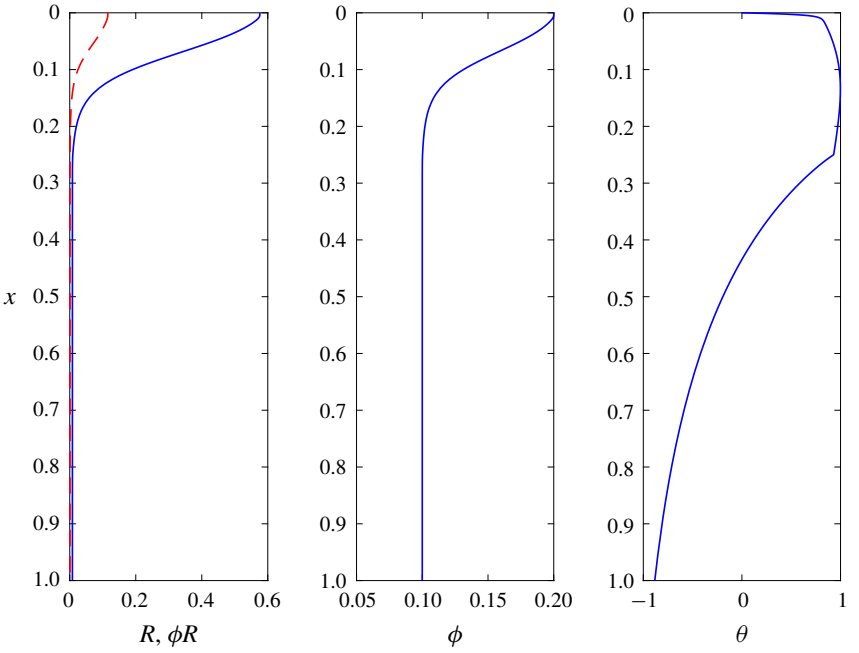

FIGURE 5. (Colour online) Solution of the inverse problem for the drawing of a preform with initial aspect ratio $\phi_{in} = 0.2$ to a fibre with aspect ratio $\phi_{out} = 0.1$ using a draw ratio of $D = 5000$ ($\chi_{out} = 0.014$), yielding $\theta_H = 1229.5$ K and $T = 24.65$. In addition $\ell = 0.25$ and the computed value of θ_H resulted in $\theta_{hot} = 965.7$ K, $Ca = 0.41$, $\mathcal{H}_C = 58.72$, $\mathcal{H}_R = 25.25$, $\vartheta_a = 0.30$ and $\vartheta_{in} = 0.67$.

Having solved for T we must find the value of θ_H consistent with it, which is needed to compute θ_{hot} used in the problem scaling. This may be done in a manner similar to that described in § 3.2, where the tension T consistent with a specified draw ratio D was determined. First, the function that solves (2.41)–(2.43) must have θ_H as the input parameter, while T is set to the known value. Then a standard root-finding procedure (such as 'fzero' in MATLAB), together with an interval in which one expects to find the value θ_H, is used to find the solution that satisfies $\tau_{stop} - \tau_{out} = 0$.

Again, as was the case for solving for a prescribed draw ratio, it is possible for the ODE solver to fail for values of θ_H used in the iterative process for which the specified fibre tension T is inappropriately large. This is again due to the stiffness of the problem. Should this occur, we use a similar procedure to that adopted in § 3.2, that is, take the effective value of τ_{stop} to be the last value computed (corresponding to an $x < 1$) and use this to compute $\tau_{stop} - \tau_{out}$. This methodology gives a robust way to obtain the desired solution.

It might be considered better to have the ODE solver compute to $\tau = \tau_{out}$ and use the root-finding procedure to find the value of θ_H corresponding to $x(\tau_{out}) = 1$; the ODE solver would not, then, need the stopping event at $x = 1$. However, a trial value of θ_H does not have to be too much smaller than the correct value for the ODE solver to take an inordinate amount of time to reach τ_{out}. This is, no doubt, related to the stiffness of the problem. Hence, while this method can work if given enough time, we have chosen to use the much faster method described above.

Figure 5 shows the solution for the drawing of a preform with initial aspect ratio $\phi_{in} = 0.2$ into a fibre with aspect ratio $\phi_{out} = 0.1$ using a draw ratio $D = 5000$ ($\chi_{out} =$

0.0141), equation (3.5) to define $\vartheta_h(x)$ to within the arbitrary parameter θ_H, and other input parameters as used previously. The tension value found for this problem was $T = 24.6453$ (6 sig. fig.) while the maximum heater temperature was determined as $\theta_H = 1229.5$ K, yielding $\theta_{hot} = 965.7$ K. Substituting the values of T and θ_H into the code of § 3.1, which uses prescribed values for these parameters, yields $D = 5000.9$ and $\phi_{out} = 0.1$, which confirms the accuracy of our method.

In the case in which the surface tension depends explicitly on temperature, one cannot explicitly solve for the tension T in terms of the draw ratio D and τ_{out}. We therefore need to simultaneously solve for θ_H and T to ensure that $\tau_{stop} - \tau_{out} = 0$ and the desired draw ratio D is obtained. This represents two equations for two unknowns which, given a good initial guess, can be solved using a standard root-finding technique. A good initial guess can be obtained by solving a system with constant surface tension as described above.

Next we return to the earlier mentioned matter of the non-uniqueness of $\vartheta_h(x)$ for a fibre draw specified by D and τ_{out}. It was shown in Stokes *et al.* (2014), for the case of constant surface tension, that the fibre tension determines the required harmonic mean of the viscosity $\mu(x)$ over the neck-down length ($0 \leqslant x \leqslant 1$), and any viscosity profile that gives the necessary harmonic mean will do (provided there are no very rapid changes of the cross-sectional area with x which would invalidate the model assumptions). Since there is not a unique viscosity profile $\mu(x)$, this implies there is not a unique temperature profile $\theta(x)$ which, in turn, implies non-uniqueness of the heater temperature profile $\theta_h(x)$ and, hence, $\vartheta_h(x)$.

We now consider how the non-uniqueness of the heater temperature profile extends to the case of non-constant surface tension. Proceeding as in Stokes *et al.* (2014) we consider viscosity μ to be a function of $\theta(x)$, but surface tension γ to be a function of $\theta(\tau)$, and so write (2.43) in the integral form

$$\int_0^x \frac{1}{\mu}\,\mathrm{d}x' = Ca \int_0^\tau \frac{1}{\gamma\chi}\,\mathrm{d}\tau'. \tag{3.13}$$

On using (3.7) to substitute for χ in (3.13) we are able to obtain an exact expression for the integral on the right-hand side so that

$$\int_0^x \frac{1}{\mu}\,\mathrm{d}x' = -\frac{1}{T}\log(H(\tau)\chi(\tau)). \tag{3.14}$$

Then, using $\chi(\tau_{out}) = 1/\sqrt{D}$ and $x(\tau_{out}) = 1$, we have

$$\int_0^1 \frac{1}{\mu}\,\mathrm{d}x = \frac{1}{T}\log\left(\frac{\sqrt{D}}{H(\tau_{out})}\right), \tag{3.15a}$$

and, noting that the left-hand side of (3.15*a*) is $1/M$, where M is the harmonic mean of the viscosity over $0 \leqslant x \leqslant 1$, we have

$$1 = \frac{M}{T}\log\left(\frac{\sqrt{D}}{H(\tau_{out})}\right). \tag{3.15b}$$

This shows that D and τ_{out} alone determine the ratio of the harmonic mean of the viscosity M to the fibre tension T. We note that this result applies for fibres of arbitrary geometry. Thus, any temperature profile $\theta(\tau)$ that yields the correct value

of M/T can be used and, as for the case of constant viscosity, there is not a unique heater temperature profile for the desired draw.

However, there is a practical difficulty in the case of temperature-dependent surface tension that does not arise for constant surface tension. As seen above, and as previously shown by Stokes *et al.* (2014), for the case of constant surface tension for which the tension T is independent of temperature θ, the temperature profile need not be explicitly solved for if the required fibre tension can be externally measured and hence tuned to the value required by the model by varying the furnace temperature. This is a very powerful result but it does not extend to the case of temperature-dependent surface tension for which temperature must be determined in order to compute the fibre tension. Moreover, the heater temperature profile $\vartheta(x)$ must be known to within a single arbitrary parameter θ_H if one is to use the model to find the fibre tension and so be able to tune to this value by varying θ_H.

If the fibre tension can be measured and the surface tension is insensitive to changes in temperature, we can avoid the thermal modelling altogether. However, for glasses with significant surface tension variation we see that the thermal modelling is critical. Moreover, it is not always experimentally possible to measure and control the fibre tension, either because the draw tower does not have the required instrumentation or because the fibre is too fragile to use it. Then the procedure described above, along with the heater temperature profile $\vartheta_h(x)$ to within an arbitrary constant θ_H, will be needed for obtaining the value of θ_H to achieve the required fibre. Thus, in either of the cases of significant temperature dependence of the surface tension or inability to measure and control fibre tension the procedure described above must be used. In addition, one must also solve the thermal problem if one requires detailed information about the geometry of the thread in the draw tower rather than just the shape at the exit.

3.4. *Inverse problem for an axisymmetric rod*

For completeness we here consider the drawing of a solid axisymmetric preform into a fibre. In this case there is no need to solve the transverse-flow model because the scaled cross-sectional geometry starts and stays a circle with no internal holes. Hence we cannot determine τ_{out} from the change in the cross-sectional geometry.

In this case

$$H(\tau) = \exp\left(-\frac{\sqrt{\pi}}{6}\tau\right), \tag{3.16}$$

$$\int_0^{\tau_{out}} H(\tau)\,\mathrm{d}\tau = \frac{6}{\sqrt{\pi}}\left(1 - \exp\left(-\frac{\sqrt{\pi}}{6}\tau_{out}\right)\right), \tag{3.17}$$

and we may, again, use (3.10) with constant γ to relate D, τ_{out} and T. For the inverse problem, D is specified and alone dictates the change in geometry (cross-sectional area) from preform to fibre. However, unlike for axisymmetric tubes, we have the flexibility to choose the value of $\tau_{out} > 0$ to correspond to a tension T that is not so large that there is significant risk of breaking the fibre, and not too small such that the viscosity of the fibre material is too low. Thus, for $D > 1$, we rearrange (3.10) to give

$$\tau_{out} = \frac{6}{\sqrt{\pi}}\log\left(\frac{6CaT/(\gamma\sqrt{\pi}) - 1/\sqrt{D}}{6CaT/(\gamma\sqrt{\pi}) - 1}\right). \tag{3.18}$$

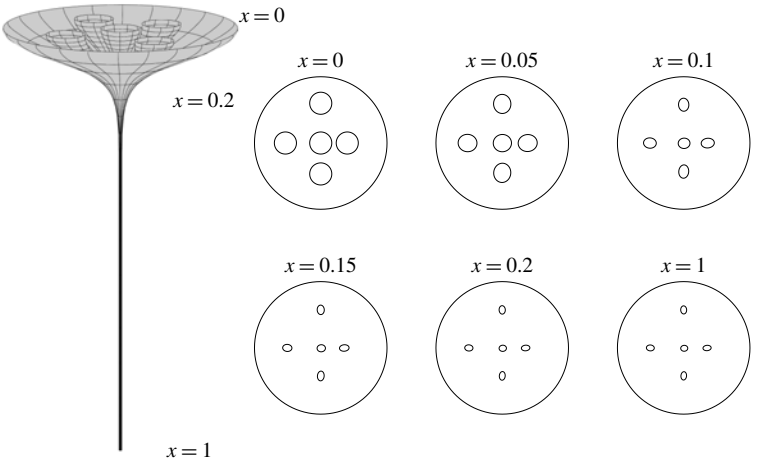

FIGURE 6. Solution of the forward problem for the drawing of a non-axisymmetric preform featuring five channels using a tension of $T = 25$ and $\vartheta(x)$ given by (3.5), resulting in $D = 5886$ ($\chi_{out} = 0.013$). The scaled cross-sectional deformation is shown for six positions between $x = 0$ and $x = 1$. The other input parameters were $Ca = 0.341$, $\mathcal{H}_C = 51.071$, $\mathcal{H}_R = 22.260$, $\ell = 0.2$, $\vartheta_a = 0.31$ and $\vartheta_{in} = 0.67$.

We then specify $T > \gamma\sqrt{\pi}/(6Ca)$ and compute τ_{out}. We can then find the required heater temperature θ_H following the same procedure that we used for axisymmetric tubes.

3.5. *Problems involving non-axisymmetric tubes*

All of the problems for axisymmetric tubes that we have described above can be generalised to the non-axisymmetric case. The only difference involves the solution of the cross-sectional geometry in terms of τ using (2.39*a*)–(2.39*f*) to obtain the functions $\tilde{\Gamma}(\tau)$ and $\tilde{\Gamma}^{(0)}(\tau)$. Once these two functions have been obtained, the techniques for the ODEs are essentially the same as the axisymmetric case. Methods for solving the evolution of the cross-sectional geometry have been discussed in detail in Stokes *et al.* (2014) and here we just mention some important points. In some special cases, pseudo-analytic solutions can be obtained using complex variable techniques, but typically the transverse-flow problem can be readily solved using spectral methods. In solving the inverse transverse-flow problem, one may need to propagate the desired shape backwards in τ. This process is inherently ill posed and regularisation of the numerical solution process may be required.

An example calculation is shown in figure 6 for the drawing of a non-axisymmetric preform with five channels. The channels are all of equal radius with the four radial channels each a different distance from the central channel. The solution to the transverse flow problem was computed via the generalised elliptical pore method of Buchak *et al.* (2015). This simulation used a prescribed tension of $T = 25$, which yields a draw ratio of $D = 5886$. The resulting deformation of the cross-sectional hole pattern is shown at six positions between $x = 0$ and $x = 1$. Under the influence of surface tension each channel shrinks in relative size and the radial channels become elliptical in shape.

4. Conclusion

In this paper, we have developed a theoretical framework that can efficiently deal with the effects of heating and cooling in the drawing of a viscous thread with an arbitrary number of internal holes of arbitrary shape. This requires the solution of a fully coupled flow and temperature model that can describe the evolution of the thread and the holes throughout the drawing process. We have used asymptotic techniques to determine a transformation that decouples the transverse aspect of the flow from the axial flow. This allows one to use standard methods to obtain the solution of a two-dimensional Stokes flow problem in the absence of axial stretching. This solution can then be substituted into a system of three ordinary differential equations that determine the nature of the transformation and hence allow one to reconstruct the flow. We have used these ideas to develop a straightforward numerical technique to solve the problem. This technique is robust, accurate and easy to implement. This is in direct contrast with solving the full three-dimensional free boundary problem that represents a daunting numerical task. Our numerical method works well even for complex geometries and in cases in which enormous variations in the viscosity occur.

We used this method to solve the problem of an axisymmetric tube pulled by a prescribed tension. In this case, the transverse flow has a simple explicit solution and the solution can be solved very efficiently and with high accuracy using a standard ODE solver. For the case of an axisymmetric tube extended using a fixed draw ratio, the problem requires the use of an ODE solver along with a simple one-dimensional root-finding procedure to determine the required fibre tension. This can also be achieved efficiently and with high accuracy. We also considered the inverse problem that involves determining the initial cross-sectional geometry, draw tension and heater temperature to obtain a desired cross-sectional shape and change in cross-sectional area at the device exit. In the case of an axisymmetric thread with constant surface tension, we derived an explicit expression for the fibre tension in terms of the draw ratio and τ_{out}, which give the change in cross-sectional area and the required preform geometry, respectively. This then allowed us to solve for the heater temperature using a simple one-dimensional root-finding procedure. In the case of temperature-dependent surface tension, one needs to simultaneously solve for the heater temperature and the fibre tension, but this can be done relatively easily given that a good initial guess can be obtained by solving a system with constant surface tension. We also showed that the methodology we have developed can be directly generalised to non-axisymmetric threads.

In summary, the transformation that we have derived in this paper represents a powerful tool in the analysis of axially extended fibres that are subjected to heating and cooling. Under the transformation the transverse flow can be decoupled from the axial flow and temperature. The solution of this transverse-flow problem provides the scaled cross-sectional boundary lengths that are required to reduce the axial flow and temperature problem into a system of three one-dimensional ODEs. This decoupling of the transverse-flow problem from the axial flow and energy equations can also be used if the thread is subjected to gravitational stretching (Tronnolone *et al.* 2016). Moreover, in the case of pressurisation of channels, where there is two-way coupling between the transverse flow and the axial flow and energy problems, the solution methods described in (Chen *et al.* 2015) may be readily employed. For smaller *Pe* flows, axial conduction may be important, making this problem significantly more difficult to solve. This case will be examined in future work.

Acknowledgements

Y.M.S. acknowledges the support of the Australian Research Council grants DP130101541 and FT160100108. J.J.W. was supported by the Research Grants Council of Hong Kong Special Administrative Region, China (CityU 11303314).

REFERENCES

BOYD, K., EBENDORFF-HEIDEPRIEM, H., MONRO, T. M. & MUNCH, J. 2012 Surface tension and viscosity measurement of optical glasses using a scanning CO_2 laser. *Opt. Mater. Express* **2** (8), 1101–1110.

BRADSHAW-HAJEK, B. H., STOKES, Y. M. & TUCK, E. O. 2004 Computation of extensional fall of slender viscous drops by a one-dimensional Eulerian method. *SIAM J. Appl. Maths.* **67**, 1166–1182.

BUCHAK, P., CROWDY, D. G., STOKES, Y. M. & EBENDORFF-HEIDEPRIEM, H. 2015 Elliptical pore regularisation of the inverse problem for microstructured optical fibre fabrication. *J. Fluid Mech.* **778**, 5–38.

CHEN, M. J., STOKES, Y. M., BUCHAK, P., CROWDY, D. G. & EBENDORFF-HEIDEPRIEM, H. 2015 Microstructured optical fibre drawing with active channel pressurisation. *J. Fluid Mech.* **783**, 137–165.

CUMMINGS, L. J. & HOWELL, P. D. 1999 On the evolution of non-axisymmetric viscous fibres with surface tension, inertia and gravity. *J. Fluid Mech.* **389**, 361–389.

DENN, M. M. 1980 Continuous drawing of liquids to form fibers. *Annu. Rev. Fluid Mech.* **12**, 365–387.

DEWYNNE, J. N., HOWELL, P. D. & WILMOTT, P. 1994 Slender viscous fibres with inertia and gravity. *Q. J. Mech. Appl. Maths* **47**, 541–555.

DEWYNNE, J. N., OCKENDON, J. R. & WILMOTT, P. 1992 A systematic derivation of the leading-order equations for extensional flows in slender geometries. *J. Fluid Mech.* **244**, 323–338.

FITT, A. D., FURUSAWA, K., MONRO, T. M., PLEASE, C. P. & RICHARDSON, D. A. 2002 The mathematical modelling of capillary drawing for holey fibre manufacture. *J. Engng Maths* **43**, 201–227.

FOREST, M. G. & ZHOU, H. 2001 Unsteady analysis of thermal glass fiber drawing processes. *Eur. J. Appl. Maths* **12**, 479–496.

GRIFFITHS, I. M. & HOWELL, P. D. 2007 The surface-tension-driven evolution of a two-dimensional annular viscous tube. *J. Fluid Mech.* **593**, 181–208.

GRIFFITHS, I. M. & HOWELL, P. D. 2008 Mathematical modelling of non-axisymmetric capillary tube drawing. *J. Fluid Mech.* **605**, 181–206.

GUPTA, G. & SCHULTZ, W. W. 1998 Non-isothermal flows of Newtonian slender glass fibers. *Intl J. Non-Linear Mech.* **33**, 151–163.

HE, D., WYLIE, J. J., HUANG, H. & MIURA, R. M. 2016 Extension of a viscous thread with temperature-dependent viscosity and surface tension. *J. Fluid Mech.* **800**, 720–752.

KAYE, A. 1991 Convected coordinates and elongational flow. *J. Non-Newtonian Fluid Mech.* **40**, 55–77.

MATOVICH, M. A. & PEARSON, J. R. A. 1969 Spinning a molten threadline. *I&EC Fundamentals* **8**, 512–520.

MODEST, M. F. 2013 *Radiative Heat Transfer*, 3rd edn. Academic Press.

SCHERER, G. W. 1992 Editorial comments on a paper by Gordon S. Fulcher. *J. Am. Ceram. Soc.* **75**, 1060–1062.

SHAH, Y. T. & PEARSON, J. R. A. 1972*a* On the stability of nonisothermal fibre spinning. *Ind. Engng Chem. Fundam.* **11**, 145–149.

SHAH, Y. T. & PEARSON, J. R. A. 1972*b* On the stability of nonisothermal fibre spinning – general case. *Ind. Engng Chem. Fundam.* **11**, 150–153.

SHARTSIS, L. & SPINNER, S. 1951 Surface tension of molten alkali silicates. *J. Res. Natl. Bur. Stand.* **46**, 385–390.

STOKES, Y. M., BRADSHAW-HAJEK, B. H. & TUCK, E. O. 2011 Extensional flow at low Reynolds number with surface tension. *J. Engng Maths* **70**, 321–331.

STOKES, Y. M., BUCHAK, P., CROWDY, D. G. & EBENDORFF-HEIDEPRIEM, H. 2014 Drawing of micro-structured optical fibres: circular and non-circular tubes. *J. Fluid Mech.* **755**, 176–203.

STOKES, Y. M. & TUCK, E. O. 2004 The role of inertia in extensional fall of a viscous drop. *J. Fluid Mech.* **498**, 205–225.

STOKES, Y. M., TUCK, E. O. & SCHWARTZ, L. W. 2000 Extensional fall of a very viscous fluid drop. *Q. J. Mech. Appl. Maths* **53**, 565–582.

SUMAN, B. & KUMAR, S. 2009 Draw ratio enhancement in nonisothermal melt spinning. *AIChE J.* **55**, 581–593.

TARONI, M., BREWARD, C. J. W., CUMMINGS, L. J. & GRIFFITHS, I. M. 2013 Asymptotic solutions of glass temperature profiles during steady optical fibre drawing. *J. Engng Maths* **80**, 1–20.

TRONNOLONE, H., STOKES, Y. M. & EBENDORFF-HEIDEPRIEM, H. 2017 Extrusion of fluid cylinders of arbitrary shape with surface tension and gravity. *J. Fluid Mech.* **810**, 127–154.

TRONNOLONE, H., STOKES, Y. M., FOO, H. T. C. & EBENDORFF-HEIDEPRIEM, H. 2016 Gravitational extension of a fluid cylinder with internal structure. *J. Fluid Mech.* **790**, 308–338.

WYLIE, J. J., BRADSHAW-HAJEK, B. H. & STOKES, Y. M. 2016 The evolution of a viscous thread pulled with a prescribed speed. *J. Fluid Mech.* **795**, 380–408.

WYLIE, J. J. & HUANG, H. 2007 Extensional flows with viscous heating. *J. Fluid Mech.* **571**, 359–370.

WYLIE, J. J., HUANG, H. & MIURA, R. M. 2007 Thermal instability in drawing viscous threads. *J. Fluid Mech.* **570**, 1–16.

WYLIE, J. J., HUANG, H. & MIURA, R. M. 2011 Stretching of viscous threads at low Reynolds numbers. *J. Fluid Mech.* **683**, 212–234.

WYLIE, J. J., HUANG, H. & MIURA, R. M. 2015 Asymptotic analysis of a viscous thread extending under gravity. *Physica* D **313**, 51–60.

YARIN, A. L. 1986 Effect of heat removal on nonsteady regimes of fiber formation. *J. Engng Phys.* **50**, 569–575.

YARIN, A. L., GOSPODINOV, P. & ROUSSINOV, V. I. 1994 Stability loss and sensitivity in hollow fiber drawing. *Phys. Fluids* **6** (4), 1454–1463.

YARIN, A. L., RUSINOV, V. I., GOSPODINOV, P. & ST. RADEV 1989 Quasi one-dimensional model of drawing of glass micro capillaries and approximate solutions. *Theor. Appl. Mech.* **20** (3), 55–62.